

Proton Flux Measurement from Neutron Monitor Data Using Neural Networks

Pengwei Zhao*

School of Physics and Astronomy, Sun Yat-sen University, Zhuhai 519082, China

Jie Feng†

School of Science, Shenzhen Campus of Sun Yat-sen University, Shenzhen 518107, China

(Dated: December 30, 2024)

Accurate measurements of cosmic ray proton flux are crucial for studying the modulation processes of cosmic rays during the solar activity cycle. We present a proton flux measurement method based on ground-based neutron monitor (NM) data and machine learning techniques. After preprocessing the NM data, we use a convolutional neural network (CNN) model to simulate the relationship between the NM observations and proton flux measured by the Alpha Magnetic Spectrometer (AMS-02). We obtain daily proton flux data ranging from 1GV to 100GV for the period from 2011 to 2024, showing that the measured values are in good agreement with the observed ones. In particular, we provide daily proton flux measurements for periods when AMS-02 data are unavailable due to operational reasons. We also perform wavelet analyses on the continuous proton flux data to investigate the relationship between proton flux and solar activity variations, particularly during late 2014 when AMS-02 measurements were missing.

Keywords: Space radiation, Convolutional neural network, Cosmic rays, Solar modulation, Wavelet analysis

I. INTRODUCTION

Cosmic rays entering the solar system are influenced by the heliospheric magnetic field, which varies with solar activity, thereby limiting the number of cosmic rays that reach Earth. These variations in the heliospheric magnetic field cause observable changes in cosmic ray intensity that correlate with solar activity.

The flux of galactic cosmic rays is inversely related to solar activity. During periods of high solar activity, marked by increased sunspot numbers, the intensity of galactic cosmic rays decreases. This pattern varies according to the 11-year sunspot cycle. Additionally, galactic cosmic rays also exhibit shorter periodic oscillations. As Ref. [1] found, there is evidence suggesting a 27-day cycle associated with solar rotation.

In addition to these periodic variations, non-recurrent perturbations are also observed that are associated with sudden solar flares. This results in a rapid change in flux over a period ranging from several hours to days. A Forbush decrease (FD) [2] is an example of such a perturbation, representing a sudden decrease in Galactic Cosmic Rays (GCRs) due to intense solar wind transients.

The above phenomena can be observed by ground-based detectors (e.g., Neutron Monitors [3]) and space-based detectors, such as the Payload for Antimatter Matter Exploration and Light-nuclei Astrophysics (PAMELA) [4], the Alpha Magnetic Spectrometer (AMS) [5], and the Dark Matter Particle Explorer (DAMPE) [6], which measure the time variation of cosmic rays.

Among them, neutron monitors are a key type of ground-based detector that provides long-term cosmic ray data for studies. After applying corrections for terrestrial factors, such as geomagnetic, atmospheric, and instrumental effects [7], these monitors detect secondary nucleons produced in the atmosphere from cascades initiated by primary cosmic-ray particles.

The measurement is related to the local geomagnetic field. A particle that can be detected by a neutron monitor must have a rigidity greater than the geomagnetic cutoff rigidity, which represents the lowest rigidity required for a particle to penetrate a given location in the magnetosphere. Geomagnetic cutoff rigidity estimates a neutron monitor's sensitivity to cosmic ray rigidity.

Since the Climax neutron monitor (NM) began operation in 1951, neutron monitors have been used to observe cosmic rays. Over time, more of these instruments have been installed worldwide [8], and currently, approximately 50 are active in the global network. The cosmic ray counts observed at each station are those with rigidity exceeding the local geomagnetic cutoff rigidity. Therefore, the recorded cosmic rays at different stations exhibit varying rigidity ranges, and the specifications, including the cutoff rigidity for each station, are detailed at <https://www.nmdb.eu/nest/>.

Despite their extensive use in monitoring cosmic ray variations, neutron monitors have certain limitations. Firstly, they measure the integrated flux of cosmic rays above the local geomagnetic cutoff rigidity (e.g., momentum per unit charge), without distinguishing between different particle species or their individual rigidities. This integration results in a combined measurement that encompasses all cosmic ray particles exceeding the cutoff threshold, therefore making it challenging to analyze specific contributions from various species or energy levels. Moreover, the cutoff rigidities of neutron monitors do

* These authors contributed equally to this work.

† E-mail: fengj77@mail.sysu.edu.cn

not reflect the actual rigidity of the cosmic ray flux, as low-energy cosmic rays do not produce enough secondary particles to reach the ground. This limitation is evident when comparing neutron monitor data with direct cosmic ray measurements, as shown in Fig. 1.

Unlike ground-based detectors, space-based detectors, such as AMS, are capable of directly detecting cosmic rays. AMS has provided detailed measurements of cosmic ray proton fluxes Φ_p between 2011 and 2019 [5]. The rigidity range spans from 1 to 100 GV and reveals periodic variations correlated with solar activity. In particular, the study highlights periodic flux variations on timescales of 27, 13.5, and 9 days, which are associated with solar rotation and the dynamics of interplanetary magnetic fields. In addition, AMS has measured the cosmic ray helium fluxes Φ_{He} during the same period [9]. The flux ratios Φ_{He}/Φ_p are around 10% and vary with Φ_p , suggesting that NM rates are likely correlated with Φ_p .

While the AMS Collaboration has provided valuable insights into cosmic ray proton flux variations, challenges such as data discontinuities caused by detector studies and upgrades from September 2014 to November 2014 and from July 2018 to October 2019 have hindered continuous periodic analysis. As a result, there have been no direct, continuous daily measurements of the rigidity dependence of the 9-day, 13.5-day, and 27-day periodicities during these periods, covering a broad range of rigidities.

Moreover, AMS daily data are insufficient for analyzing short-duration cosmic ray variations, such as FDs. Higher time resolution data, such as hourly data, are needed to address this. Fortunately, neutron monitors provide continuous measurements with higher time resolution. Our work uses machine learning techniques to calculate proton flux in space from ground-based neutron monitor data.

In this study, we employ machine learning techniques to investigate the intrinsic relationship between NM data and AMS data, thereby enabling the calculation of proton flux from NM data over the period from 2011 to 2024. This study is divided into two primary phases: NM data imputation and proton flux prediction.

In the NM data imputation phase, given that the data from individual neutron monitoring stations are independently and identically distributed, missing values often arise due to various factors, such as instrumental failures or upgrades to the neutron monitor. Consequently, the preprocessed NM data are complemented through two advanced time-series imputation algorithms. Specifically, a series of preprocessing steps are first applied to the NM data, including outlier removal, data normalization, etc. Subsequently, we employ two deep learning models, SAITS [10] and iTransformer [11], to train and optimize the preprocessed NM data, further predicting and imputing missing values.

In the second phase, leveraging the robust feature extraction capabilities of convolutional neural networks (CNNs), we train a CNN to learn the features of the completed NM data, aiming to predict the daily proton flux

in the AMS data across various rigidity intervals. Experimental results demonstrate that the trained CNN model effectively captures the latent relationship between NM data and AMS proton flux.

In terms of application, since NM data provides high-resolution input to the CNN, our approach can produce high time-resolution AMS proton flux data, such as hourly flux data, by utilizing the corresponding high time-resolution NM data. This capability is particularly advantageous for studying phenomena like FDs, which are linked to Interplanetary Coronal Mass Ejections (ICMEs) and Corotating Interaction Regions (CIRs) [12].

The unusual polar field reversal during Solar Cycle 24 is a critical phenomenon for understanding the dynamics of solar magnetic fields and their hemispheric asymmetries. However, AMS measurements during this period suffer from data gaps, which hinder comprehensive analysis and prevent the application of wavelet analysis to study periodicities, as done for other continuous time intervals.

To address this challenge, our work reconstructs the missing data for AMS from this period, creating a continuous dataset. Thanks to the high accuracy of our proposed imputation method, this reconstruction enables more detailed and accurate studies of the unusual polar field reversal, including wavelet analyses, contributing significantly to the understanding of solar and heliospheric processes during this period.

This paper is organized as follows: In Section II A, we introduce the dataset used in our analysis, detailing the sources and properties of both NM and AMS data. Our proposed framework is presented in Section II B, covering time-series imputation for NM data and proton flux prediction for AMS data. We describe our experimental results in Section III, summarize our findings, and suggest potential avenues for future research in Section IV.

II. METHODOLOGY

The cosmic ray proton flux is intrinsically correlated with neutron monitor counts, as high-energy cosmic ray protons interact with Earth's atmosphere, producing secondary particle showers. These showers, in turn, generate nucleons, which are detected by neutron monitors. Several factors influence the neutron monitor counts, including the atmospheric pressure, the cross sections of particle interactions, and the specific characteristics of the showers. To account for these complex interactions and to simplify the calculation of the relevant processes, we employ Convolutional Neural Networks (CNNs). CNNs are well-suited for modeling the nonlinear relationship between cosmic ray proton flux and neutron monitor data, enabling the efficient extraction of meaningful patterns and the adjustment for external variables, such as air pressure and cross-sectional variations, which affect the measurements.

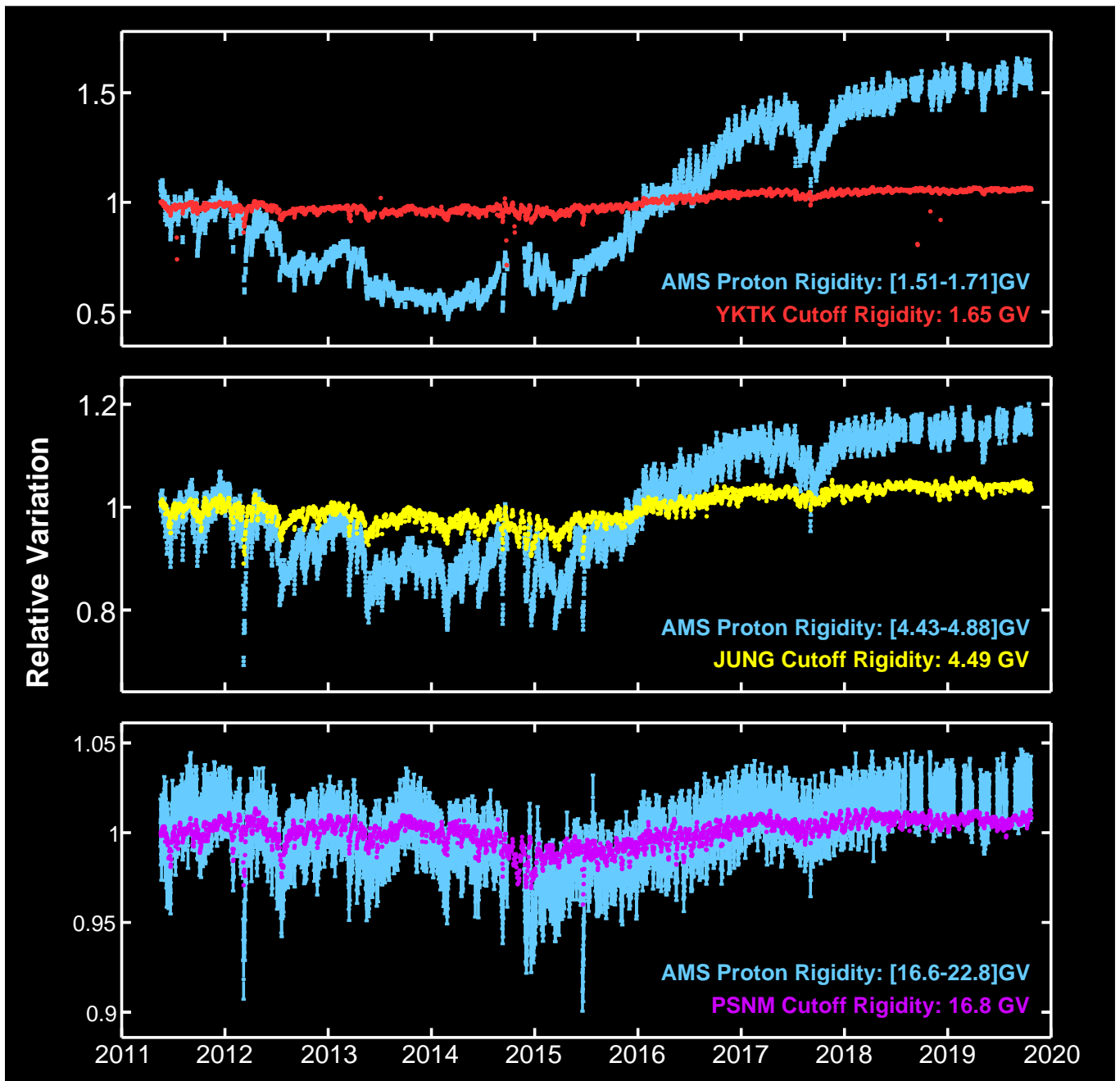


FIG. 1. The relative variations of the AMS proton flux in three different rigidity ranges compared with those of the rate reported by neutron monitors with the corresponding geomagnetic cutoff rigidities: YKTK (top), JUNG (middle), and PSNM (bottom). Both the AMS proton flux and the neutron monitor rates are normalized by their mean values. The rates of neutron monitors show different behaviors with respect to the AMS proton fluxes at close rigidities.

A. Dataset

1. Neutron Monitor Data

The neutron monitor data used in this study are obtained from the Neutron Monitor Database (NMDB) <https://www.nmdb.eu>, which compiles measurements from over 50 stations worldwide, covering a wide range

of longitudes and latitudes. Neutron monitors measure cosmic ray flux, which varies across stations due to differences in geomagnetic cutoff rigidity. The rigidity values for these stations range from 0.01 GV (e.g., Terre Adélie, Antarctica) to 16.8 GV (e.g., Princess Sirindhorn Neutron Monitor, Thailand). This study uses data spanning from January 1, 2011, to August 1, 2024.

Although NMDB provides daily data, gaps and outliers

in the dataset require additional preprocessing. Thus, we collect data from each station at higher time resolutions (e.g., 10-minute intervals, 30-minute intervals) over this period. To match the daily resolution of AMS data and ensure uniform time intervals, neutron monitor data are processed to derive daily counts.

Each station’s daily count rate is calculated by averaging valid data points, defined as recorded measurements after outlier removal using the Interquartile Range method. Outliers related to solar activity, such as FDs and Solar Energetic Particles (SEPs), are retained by comparing data from stations with similar geomagnetic cutoff rigidity. Relevant events are preserved to ensure significant signals are not mistakenly excluded as anomalies.

Further details on the NM data preprocessing steps are provided in Appendix A. The processed daily data from each station are concatenated column-wise to construct the neutron monitor dataset. To ensure dataset reliability, stations with more than 30 consecutive days of missing data are excluded from our experiments. After the filtering process, 18 stations are included in the following analysis: AATB, APTY, FSMT, INVK, JUNG, JUNG1, LMKS, MXCO, NAIN, NEWK, OULU, PSNM, PWNK, SOPB, SOPO, TERA, THUL and YKTK.

By applying the preprocessing and the filtering processes for the NM data, there are still some short time data gap in the rest 18 stations. In order to solve the missing data problem in the NM data, two advanced time-series imputation algorithms are utilized to complement those missing values. More details about two advanced time-series imputation algorithms are mentioned in Section II B.

2. Alpha Magnetic Spectrometer Data

The Alpha Magnetic Spectrometer (AMS) is a particle detector mounted on the International Space Station (ISS). Since its installation in May 2011, it has accumulated 13 years of cosmic ray data. The dataset used in this study includes proton flux measurements collected by AMS from May 20, 2011, to October 29, 2019, covering 8.5 years (2,824 days or 114 Bartels Rotation cycles) [5]. AMS recorded a total of 5.5×10^9 protons, with flux measurements spanning from 1.00 to 100 GV across 30 rigidity ranges. The data cover the ascending, maximum, and descending phases of solar cycle 24, offering a comprehensive view of cosmic ray behavior throughout the cycle.

The daily proton flux data used in this study are available on the AMS website <https://ams02.space/publications/202105>. This AMS dataset is the first to conduct a periodicity analysis across multiple rigidities, including 9-day, 13.5-day, and 27-day periodicities. To ensure data accuracy, the AMS collaboration excluded measurements affected by SEPs with rigidity below 3 GV (from 1.00 to 2.97 GV) across 9 rigidity bins. Addition-

ally, some dates in the published flux data are missing due to detector studies and upgrades [5].

B. Our Proposed Framework

1. NM Data Imputation

After the preprocessing described in Section II A, the preprocessed NM data still retains some missing values. These partially-observed time series have become a significant barrier to further analysis and modeling endeavors. To address this issue, we employ two advanced time-series imputation algorithms, SAITS [10] and iTransformer [11], to effectively complete the missing data. Leveraging the efficient integration of time-series imputation methods provided by PyPOTS [13], we implement and compare the imputation performance of various models within a unified framework, subsequently selecting two models with comparable effectiveness for in-depth discussion and analysis.

The key concept of SAITS is to utilize the Self-Attention mechanism to accurately capture the complex interdependencies between different time steps in multivariate time series. Even in environments with missing values, SAITS can realistically reconstruct the original data distribution. In this context, the model simultaneously optimizes the reconstruction of observed data and the prediction of intentionally masked values. This dual optimization ensures precise fitting of the visible data and embeds the capability to infer potential missing values within its deep feature representations.

In contrast, iTransformer, based on the Transformer architecture, aims to enhance feature extraction capabilities by learning dependencies among sequences. However, iTransformer initially lacked the capability to directly handle partially-observed time series. To overcome this limitation, the PyPOTS toolbox adopts data embedding and training strategies consistent with those of SAITS, thereby modifying iTransformer to accommodate multivariate time series with missing values as input. Through this adaptation process, iTransformer retains its feature extraction capabilities while also acquiring enhanced abilities to fill in missing values, thus enabling a fair comparison within the same dataset scenarios as SAITS.

During the data preparation phase, the original multivariate time series is divided into three datasets: 80% for the training set, 10% for the validation set, and 10% for the test set. It is noteworthy that, to further evaluate the models’ generalization performance and robustness, we employ the Missing Completely At Random (MCAR) strategy to randomly mask 30% of the observed values in both the validation and test sets. This configuration effectively simulates unknown missing scenarios encountered in real-world applications, thereby providing a rigorous and robust experimental condition for model evaluation. The masked values retained in the validation

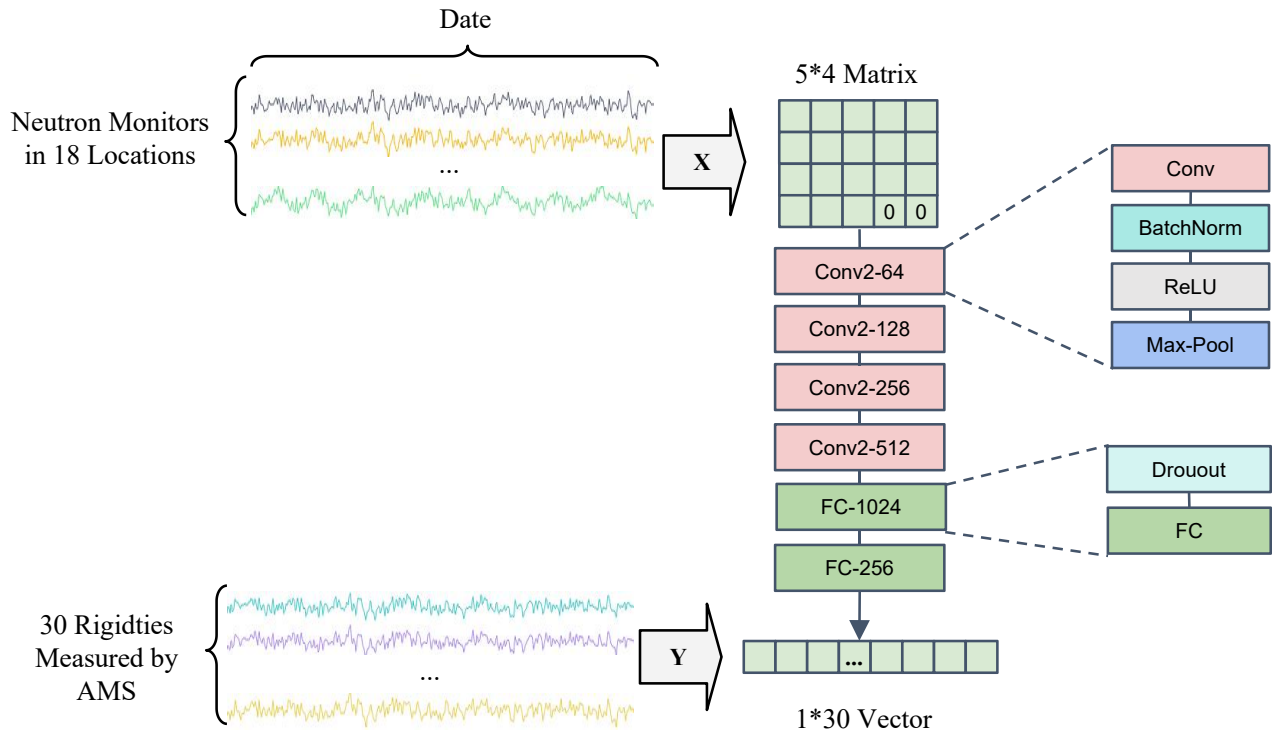


FIG. 2. Illustration of the workflow for proton flux prediction and the architecture of the CNN.

and test sets serve as ground truth data, requiring that the trained imputation model not only restore the original missing values during the evaluation phase but also demonstrate superior imputation capabilities within the simulated missing environment. Finally, the completed NM data will be utilized as input for predicting the daily proton flux in the AMS data across various rigidity intervals.

2. Proton Flux Prediction

In this study, we aim to establish the relationship between NM data and proton flux. Therefore, we align the completed NM data with AMS data by date, thereby creating a paired NM-AMS dataset that serves as input and output for training predicted models. Specifically, the input data encompasses complete NM data from May 20, 2011, to October 29, 2019, featuring 18 input variables, each corresponding to data from an individual neutron monitor station. The model output represents the daily proton flux measured by AMS across various rigidity intervals for the same time period.

Given the capability of CNN to efficiently extract features through convolutional kernels, we pad the input features with two zeros at the end to form a 4×5 input matrix. We design 4 convolutional layers utilizing 2×2 convolutional kernels for feature extraction, complemented by 2 fully connected layers for subsequent processing. To mitigate overfitting, dropout [14] layers are

incorporated within each fully connected layer. Additionally, batch normalization [15] is employed in the convolutional layers to enhance the training stability and convergence speed of the model. The architecture of the CNN and the workflow for proton flux prediction are illustrated in FIG 2.

In the experiment, in addition to employing dropout layers, we implement an early stopping [16] strategy to further prevent overfitting. The paired NM-AMS dataset is randomly partitioned into three subsets, with 90% for the training set, 5% for the validation set, and 5% for the test set. We set the batch size to 256 and the learning rate to 1×10^{-3} . When the performance on the validation set does not improve over 30 consecutive training epochs, the learning rate is automatically reduced by a factor of 0.1 until it reached a minimum value of 1×10^{-6} , at which point the adjustment process ceased. Furthermore, inspired by ensemble learning principles, we generate 5 independent models using 5 different random seeds and average the predictions from these models to form the final output. This approach helps reduce fluctuations caused by individual models, thereby enhancing the robustness of the predictive model.

We evaluate the performance of the time series imputation methods the predictive models using Mean Absolute Error (MAE), Root Mean Square Error (RMSE) and R^2 . MAE and RMSE are calculated using the formulas:

$$\text{MAE} = \frac{1}{n} \sum_{i=1}^n |y_i - \hat{y}_i| \quad (1)$$

$$\text{RMSE} = \sqrt{\frac{1}{n} \sum_{i=1}^n (y_i - \hat{y}_i)^2} \quad (2)$$

where y_i represents the true value and \hat{y}_i denotes the predicted value for the i^{th} observation. The coefficient of determination, R^2 , is defined by the formula:

$$R^2 = 1 - \frac{\sum_{i=1}^n (y_i - \hat{y}_i)^2}{\sum_{i=1}^n (y_i - \bar{y})^2} \quad (3)$$

where \bar{y} is the mean of the observed data, indicating how well the predicted values approximate the actual data points. A higher R^2 value signifies a better fit of the model to the observed data, with values ranging from 0 to 1, where values closer to 1 denote superior model performance.

III. RESULTS

A. Missing Data Imputation Performance

We compare the imputation performance of various models within a unified framework on the NM dataset. The performance comparison results are shown in Table I. In this experiment, the results indicate that both SAITS and iTransformer outperform TimesNet and Transformer in terms of MAE and RMSE. While SAITS, Transformer, and iTransformer fundamentally rely on self-attention mechanisms to model temporal sequences, TimesNet adopts a different approach by transforming time series signals into two-dimensional time-frequency representations and employing a multi-scale modeling paradigm. These findings suggest that self-attention-based methods are more adept at extracting intricate temporal and spectral features inherent in the NM data. Moreover, when compared to the Transformer architecture, the enhanced iTransformer and SAITS exhibit greater efficiency in capturing subtle time-dependent patterns, thereby achieving improved performance. More details of the imputation results and visualizations are shown in Figure 5 in Appendix B.

TABLE I. Performance comparisons of four time series imputation methods on the NM dataset.

Method	MAE (\downarrow)	RMSE (\downarrow)
TimesNet [17]	0.0695	0.0845
Transformer [18]	0.0247	0.0422
iTransformer	0.0190	0.0289
SAITS	0.0158	0.0294

B. Proton Flux Prediction Performance

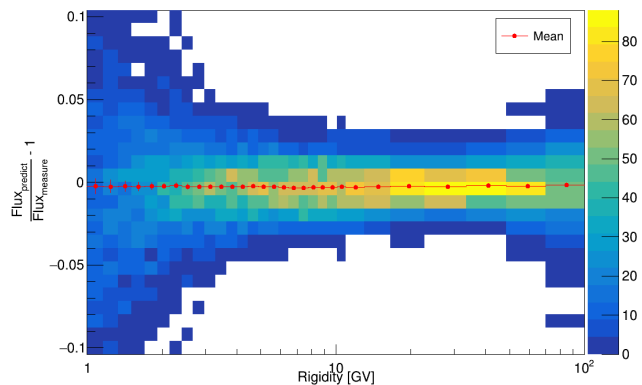


FIG. 3. Distribution of $[(\text{Flux}_{\text{predicted}}/\text{Flux}_{\text{measured}}) - 1]$. The histogram illustrates the distribution across different rigidity bins. The red dots represent the mean value for each rigidity bin. The mean being close to 1 indicates that the predicted flux values are approximately equal to the measured flux values, demonstrating that the results calculated with our CNN model closely match the observed data.

To evaluate the accuracy of our CNN model, we calculate the ratio between the proton flux measured by our model and the AMS measurements for each rigidity bin, expressed as $[(\text{Flux}_{\text{model measured}}/\text{Flux}_{\text{AMS observed}}) - 1]$. A close agreement between the model-measured and AMS-observed values indicates good model performance. The results, shown in FIG 3, display the distribution of this ratio across different rigidity bins. These results demonstrate that the proton flux measured by our CNN model aligns well with the AMS measurements across multiple rigidity bins. However, the performance quality varies across different rigidity ranges. We hypothesize that this variation is due to the different magnitudes and error levels of cosmic ray flux at various rigidities.

C. Wavelet of AMS data

To analyze the periodicity of the proton flux, we apply wavelet analysis to detect periodic components at different time scales. The proton flux data, obtained through the method described earlier, provides a detailed understanding of its temporal behavior.

Wavelet analysis involves using a wavelet with a consistent shape, while its scale (or size) varies depending on the window size. This approach enables the detection of both short-term and long-term periodicities in the proton flux.

In our analysis, the time series X_t represents the proton flux x_n at each time index n , with the data sampled at a constant time interval δt , corresponding to one day. The wavelet transform $W_n(s)$ is then computed as the convolution of the wavelet function ψ with the proton

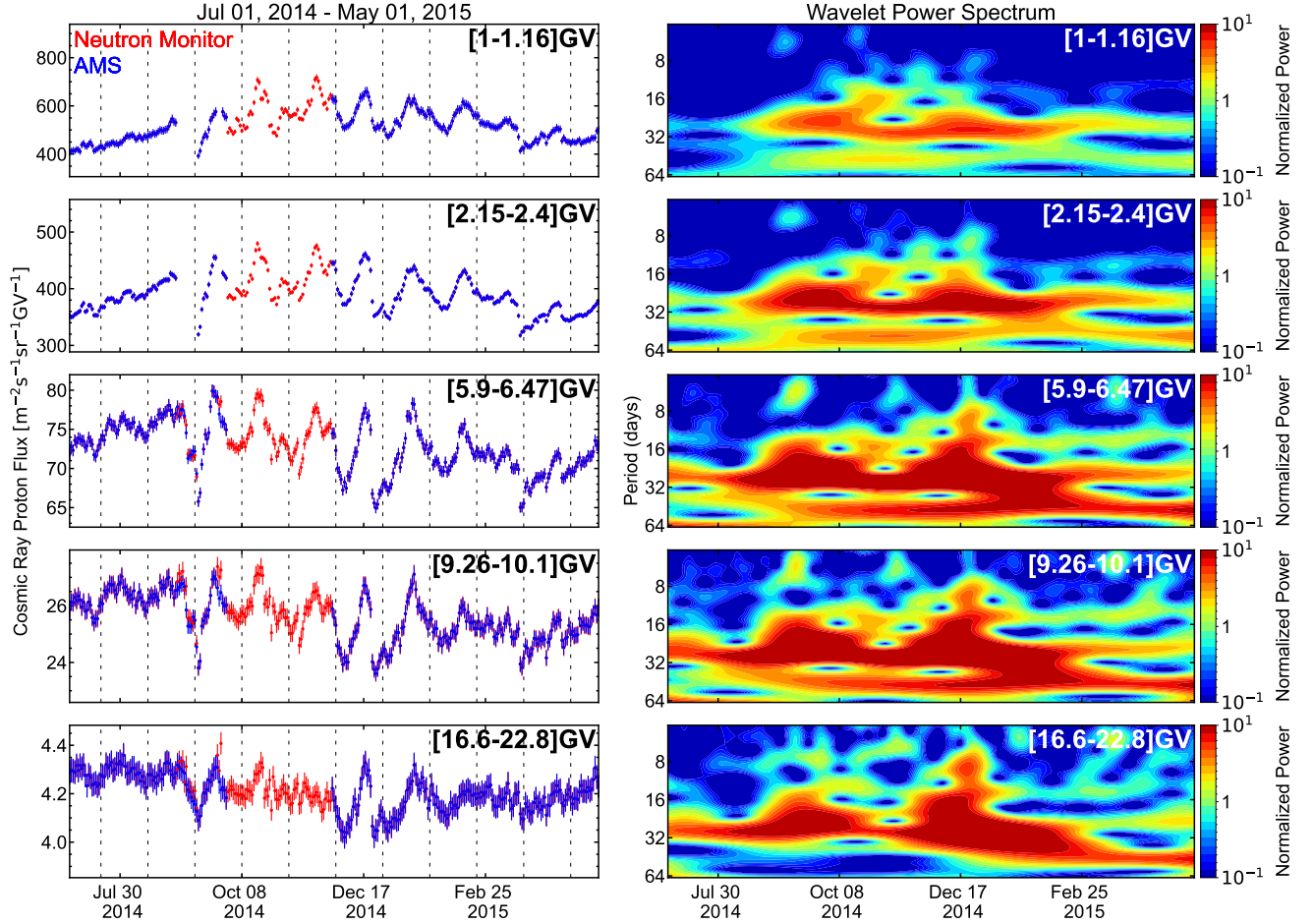


FIG. 4. The left plot shows daily cosmic ray proton flux measurements over five rigidity ranges, from low to high, plotted between July 1, 2014 and May 1, 2015. Neutron monitor measurements are shown in red, while AMS measurements are shown as blue points for comparison. Vertical dashed lines indicate the boundaries of the Bartels rotations. The right plot shows the wavelet time-frequency power spectrum corresponding to the same rigidity ranges as the neutron monitor measurements (red points in left plot). The color scale represents the normalized power.

flux time series x_n :

$$W_n(s) = \sum_{n'=0}^{N-1} x_{n'} \psi^* \left[\frac{(n' - n)\delta t}{s} \right] \quad (4)$$

where wavelet function ψ is defined as

$$\psi \left[\frac{(n' - n)\delta t}{s} \right] = \left(\frac{\delta t}{s} \right)^{1/2} \psi_0 \left[\frac{(n' - n)\delta t}{s} \right] \quad (5)$$

and the asterisk (*) indicates the complex conjugate. ψ is a scaled and time-shifted form of the mother wavelet ψ_0 , which will be defined later. The scale is adjusted by the dilation parameter s , and the wavelet is shifted in time according to the translation parameter n . The factor $s^{1/2}$ used as a normalization to keep the total energy of the scaled wavelet constant, ensuring that the shape of the

wavelet remains consistent while its size changes with the scale.

In this work, the mother wavelet ψ_0 we use is the Morlet wavelet, which is defined as the product of a complex exponential wave and a Gaussian envelope:

$$\psi_0(\eta) = \pi^{-1/4} e^{i\omega_0\eta} e^{-\eta^2/2} \quad (6)$$

where η is the non-dimensional time, and ω_0 is the wave number, and in this study we set it to 6.

In this study, we mainly choose five bins for rigidity, ranging from low to high: [1.0, 1.16] GV, [2.15, 2.4] GV, [5.9, 6.47] GV, [9.26, 10.1] GV, and [16.6, 22.8] GV.

Within the analysis, the data are standardized using the z-score, which means they are standardized by subtracting the average from the proton flux data and then dividing by the standard deviation. This process is performed to achieve uniform scaling across all levels of rigidity.

The continuous wavelet transform decomposes the proton flux time series in both time and frequency domains, yielding a wavelet power spectrum, showing the amplitude of oscillations at various periods. This allows us to detect the dominant periodicities in the data, revealing how the periodic behavior of proton flux evolves over time.

To assess the significance of the identified cycles, we compute the global wavelet spectrum, which provides a time-averaged representation of the wavelet power over the entire time series. We also compute the 95% confidence level to ensure that we can distinguish significant periodic features from background noise. This is achieved by calculating the variance of the proton flux time series and using it to compute the confidence level, as outlined in [19].

Initially, we calculate the periodicity for the entire dataset ranging from 2011 to 2024. However, since we are particularly interested in the periodicity during the exceptional polar field reversal of Solar Cycle 24, we primarily present the analysis results for this specific period, as shown in the figure.

The results of the wavelet analysis are visualized by plotting the time series of proton flux alongside the wavelet power spectrum. For each rigidity bin, we plot the proton flux time series along with the global wavelet power. This allows us to visually compare the oscillatory behavior across different energy levels and time periods, providing valuable insights into the time-varying characteristics of cosmic ray flux.

IV. CONCLUSION

We present a proton flux measurement method based on ground-based neutron monitoring station (NM) data and machine learning techniques. After preprocessing the NM data through a convolutional neural network (CNN) model, we simulate the relationship between NM observations and proton flux measured by the Alpha Magnetic Spectrometer (AMS-02). We obtain daily proton flux data for the period from 2011 to 2024, which shows that the measured values are in good agreement with the observed values. We also perform wavelet analyses of the obtained continuous proton flux data to study the relationship between proton flux and the variation in solar activity.

ACKNOWLEDGMENTS

We acknowledge the NMDB database <https://www.nmdb.eu>, founded under the European Union’s FP7 programme (contract no. 213007) for providing data. Python wavelet software provided by Evgeniya Predybaylo based on Torrence & Compo (1998)[19] and is available at <http://atoc.colorado.edu/research/>

[wavelets/](#). We are grateful for the fruitful discussions about physics and code with Junhua Li.

Appendix A: Details of Neutron Monitor Data Pre-Processing

The Neutron Monitor Database (NMDB) provides access to measurements from neutron monitor stations located worldwide, encompassing data from 58 stations. NMDB offers raw counts as well as pressure- and efficiency-corrected count rates. For our study, we select pressure- and efficiency-corrected data, which include corrections for atmospheric pressure variations and other station-specific factors (e.g., changes in infrastructure, the number or type of tubes, or registration systems). This choice ensures higher accuracy in the derived results.

Since our analysis requires daily-resolution data and the quality of neutron monitor data varies between stations, we opt to use higher-resolution data at 10-minute intervals. This provides 144 data points per day. Data points that deviate significantly from others within the same day are considered outliers and removed. The remaining data points are then used to calculate the daily count rate.

To identify and remove outliers, we employ the Interquartile Range (IQR) method. The steps are as follows:

1. Calculate the first quartile (Q1) and third quartile (Q3), which represent the 25th and 75th percentiles of the data, respectively.
2. Compute the IQR as the difference between Q3 and Q1: $IQR = Q3 - Q1$.
3. Define normal values as those within the range $[Q1 - 3.0 \times IQR, Q3 + 3.0 \times IQR]$.
4. Flag values outside this range as outliers and exclude them.

After removing outliers from the high-resolution data, the daily count rate is calculated as the mean of the remaining data points. The IQR method is reapplied to the daily-resolution data to ensure that any remaining anomalies not identified in the previous step are effectively excluded.

Besides, we make an exception for specific outliers related to solar activity, such as FDs. These events are caused by solar flares and coronal mass ejections, which increase the local magnetic field near Earth and reduce the cosmic ray flux. Since solar events tend to affect stations with similar geomagnetic cutoff rigidity [20, 21], we compare outliers across stations with similar rigidity. Outliers corresponding to the same solar event are restored, while those unrelated to solar activity remain excluded.

This process ensures a final dataset free from unrelated outliers while retaining those influenced by significant solar events, maintaining the integrity and accuracy of the analysis.

Appendix B: Imputation Results of Different Neutron Monitor Stations

In Figure 5, both SAITS and iTransformer successfully captured the underlying periodic patterns and temporal trends present in the raw neutron monitor data, with high fidelity to the original signal characteristics. The imputed values (shown in different colors) closely align with the observed measurements, indicating robust per-

formance in reconstructing missing temporal segments while preserving the intrinsic cyclical variations in cosmic ray intensity.

The imputation results in Figure 5 of AATB station further highlight the differences between SAITS and iTransformer. iTransformer is more sensitive to outliers while SAITS is not. Their differing feature extraction methods cause iTransformer to easily learn anomalous patterns from past time points, while SAITS demonstrates greater robustness. This explains why the predicted points from SAITS are more concentrated, whereas the predicted points from iTransformer are more dispersed. Although their performance metrics (mentioned in Table I) are very close, as shown in Figure 5, SAITS better meets the objectives of this work.

-
- [1] A. T. Monk and A. H. Compton, Recurrence phenomena in cosmic-ray intensity, *Reviews of Modern Physics* **11**, 173 (1939).
 - [2] J. A. Lockwood, Forbush Decreases in the Cosmic Radiation, *Space Science Reviews* **12**, 658 (1971).
 - [3] H. Moraal and P. H. Stoker, Long-term neutron monitor observations and the 2009 cosmic ray maximum, *Journal of Geophysical Research (Space Physics)* **115**, A12109 (2010).
 - [4] O. Adriani *et al.*, Time Dependence of the Electron and Positron Components of the Cosmic Radiation Measured by the PAMELA Experiment between July 2006 and December 2015, *Phys. Rev. Lett.* **116**, 241105 (2016), arXiv:1606.08626 [astro-ph.HE].
 - [5] AMS Collaboration, Periodicities in the Daily Proton Fluxes from 2011 to 2019 Measured by the Alpha Magnetic Spectrometer on the International Space Station from 1 to 100 GV, *Physical review letters* **127**, 271102 (2021).
 - [6] DAmpe Collaboration, Observations of Forbush Decreases of Cosmic-Ray Electrons and Positrons with the Dark Matter Particle Explorer, *The Astrophysical Journal Letters* **920**, L43 (2021), arXiv:2110.00123 [astro-ph.HE].
 - [7] P. Väisänen, I. Usoskin, and K. Mursula, Seven Decades of Neutron Monitors (1951-2019): Overview and Evaluation of Data Sources, *Journal of Geophysical Research (Space Physics)* **126**, e28941 (2021).
 - [8] H. Moraal, A. Belov, and J. M. Clem, Design and co-Ordination of Multi-Station International Neutron Monitor Networks, *Space Science Reviews* **93**, 285 (2000).
 - [9] M. Aguilar *et al.* (AMS), Properties of Daily Helium Fluxes, *Phys. Rev. Lett.* **128**, 231102 (2022).
 - [10] W. Du, D. Côté, and Y. Liu, Saits: Self-attention-based imputation for time series, *Expert Systems with Applications* **219**, 119619 (2023).
 - [11] Y. Liu, T. Hu, H. Zhang, H. Wu, S. Wang, L. Ma, and M. Long, itransformer: Inverted transformers are effective for time series forecasting, *arXiv preprint arXiv:2310.06625* (2023).
 - [12] S. Wang, V. Bindi, C. Consolandi, C. Corti, C. Light, N. Nikonov, and A. Kuhlman, Properties of Forbush Decreases with AMS-02 Daily Proton Flux Data, *The Astrophysical Journal* **950**, 23 (2023).
 - [13] W. Du, PyPOTS: a Python toolbox for data mining on Partially-Observed Time Series, *arXiv preprint arXiv:2305.18811* (2023).
 - [14] N. Srivastava, G. Hinton, A. Krizhevsky, I. Sutskever, and R. Salakhutdinov, Dropout: a simple way to prevent neural networks from overfitting, *The journal of machine learning research* **15**, 1929 (2014).
 - [15] S. Ioffe, Batch normalization: Accelerating deep network training by reducing internal covariate shift, *arXiv preprint arXiv:1502.03167* (2015).
 - [16] Y. Yao, L. Rosasco, and A. Caponnetto, On early stopping in gradient descent learning, *Constructive Approximation* **26**, 289 (2007).
 - [17] H. Wu, T. Hu, Y. Liu, H. Zhou, J. Wang, and M. Long, Timesnet: Temporal 2d-variation modeling for general time series analysis, *arXiv preprint arXiv:2210.02186* (2022).
 - [18] A. Vaswani, Attention is all you need, *Advances in Neural Information Processing Systems* (2017).
 - [19] C. Torrence and G. P. Compo, A Practical Guide to Wavelet Analysis., *Bulletin of the American Meteorological Society* **79**, 61 (1998).
 - [20] B. T. Kress, M. K. Hudson, R. S. Selesnick, C. J. Mertens, and M. Engel, Modeling geomagnetic cutoffs for space weather applications, *Journal of Geophysical Research (Space Physics)* **120**, 5694 (2015).
 - [21] D. F. Smart and M. A. Shea, The space-developed dynamic vertical cutoff rigidity model and its applicability to aircraft radiation dose, *Advances in Space Research* **32**, 103 (2003).

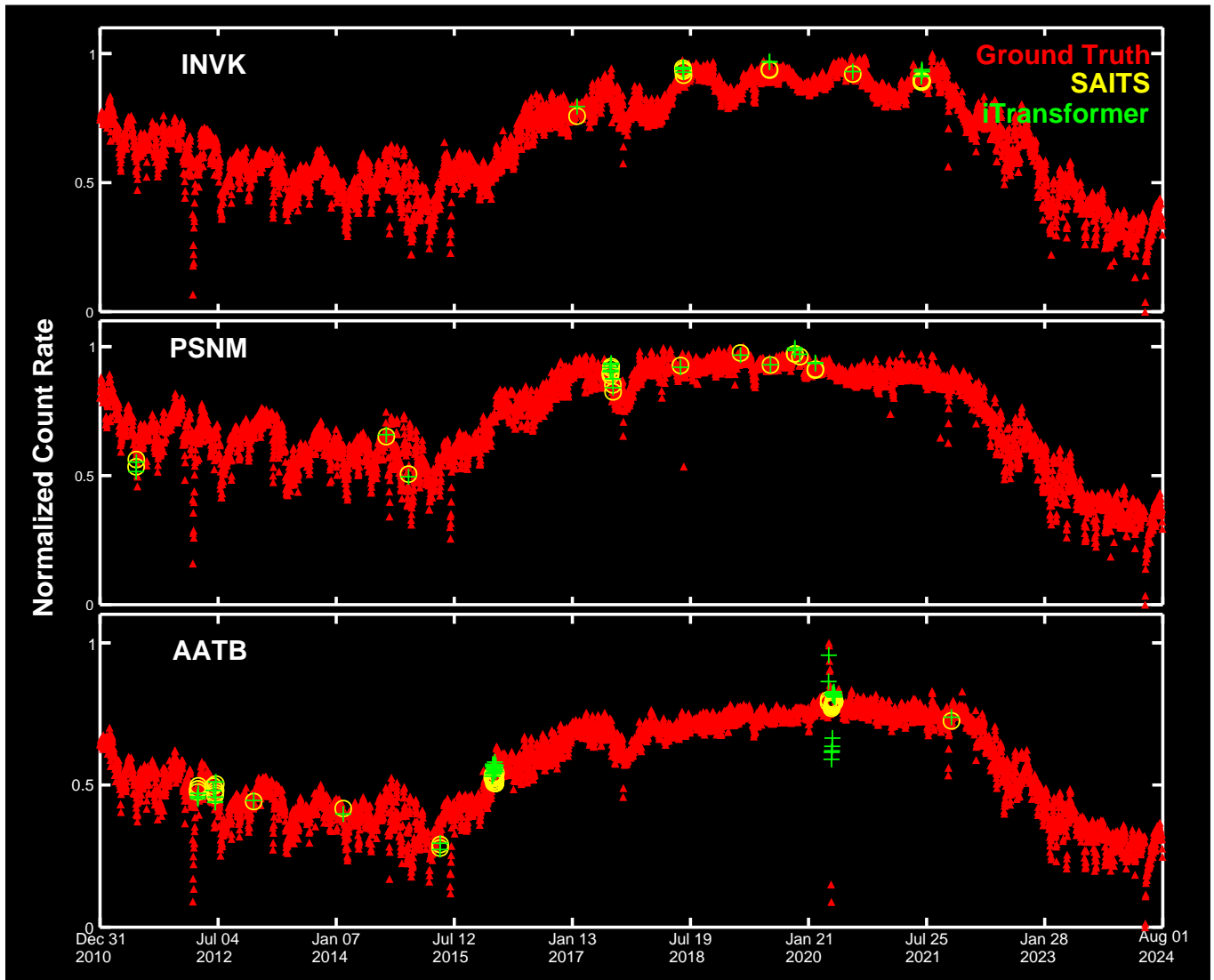


FIG. 5. Comparative imputation performance of SAITS and iTransformer models on temporal cosmic ray flux data from the INVK (Top), PSNM (Middle) and AATB (Bottom) NM stations. The normalized count rate (y-axis) is plotted against time periods (x-axis), demonstrating the reconstruction capabilities of both imputation methodologies.